Semi-Discrete Finite Element Method Analysis of Arbitrary Microstrip Elements—Static Solution

Marat Davidovitz, *Member, IEEE*, and Zhiqiang Wu, *Student Member, IEEE*

Abstract—**The Semi-Discrete Finite Element Method is applied to solve the Poisson equation for a class of microstrip structures. This numerical technique is a variant of the conventional Finite Element Method. Its name stems from the fact that finite element approximation is implemented only along two of the Cartesian coordinates, while the solution dependence on the third is handled analytically. When applicable, this method is simpler and more economical then the conventional fully-discrete version. Convergence properties of the solution are examined, and its validity tested for a number of geometries through comparison with other solutions and published data.**

I. Introduction

IN MANY situations of practical interest, particularly at lower frequencies, planar microstrip circuits can be accurately represented by lumped circuit models derived on the basis of static analysis. Capacitances associated with such models can be determined by solving, in most cases numerically, an appropriate boundary value problem for the Poisson equation. A variety of formulations and numerical treatments have been employed in microstrip capacitance calculations in the past [1]–[8].

In one possible approach to microstrip circuit modeling, the governing partial differential equations are discretized by means of the finite difference and the finite element methods, and their variants. Particularly relevant to the subject of this paper is the Method of Lines (MOL) [7], which is a semi-discrete variant of the finite difference method. In the Method of Lines discretization is introduced only along two of the Cartesian coordinate directions, thereby transforming the original set of partial differential equations into a set of coupled Ordinary Differential Equations (ODE). This set of equations can be solved analytically in most cases of interest. Consequently, the computational burden, including CPU time and storage requirements, is considerably reduced in comparison with classical finite difference schemes. An extensive review of the MOL applications, including the contributions by Pregla, Shulz, Diestel, Worm, and others can be found in [7].

In this paper a Semi-Discrete Finite Element Method (SDFEM) [9], [10] is described and applied to calculate the capacitance of microstrip patches. This method is the finite element analogue of the MOL. Although the partial discretization approach is common to both the MOL and the SDFEM, their analytical and numerical characteristics are different. Specifically:

1. The discretization in the SDFEM is not limited to rectangular grids. The domain can be divided into elements of varying sizes, orientations and shapes. Thus, arbitrary microstrip structures can be modeled very accurately.
2. Finite element methodology facilitates the use of unstructured meshes and higher-order polynomial approximations. Computer algorithms based on these techniques yield simple, yet generally applicable, software.
3. Since finite element meshes are not tied to specific grids, they are amenable to local refinement.
4. In applying the MOL to thin microstrip elements, nodes adjacent to microstrip boundaries are constrained to specific locations in order to satisfy the edge-condition. Transition conditions at dielectric boundaries also require special treatment. In certain SDFEM formulations, such constraints can be incorporated without the need for special treatment.

In Section II of this paper an SDFEM analysis of the Poisson equation for microstrip structures is presented. The mathematical statement of the boundary value problem is given in the first part of the section. A weak or variational form of the Poisson equation, to be used as the basis for the SDFEM method analysis, is introduced. The finite element methodology is used to discretize the weak formulation, reducing the problem to a set of coupled ODE. A technique for solving the ODE set by employing a transmission line analogy is described. Throughout the derivation of microstrip geometry remaines arbitrary.

Computer implementation of the solution is discussed and numerical results are presented in Section III. The choice of the basis functions used in computing the results, methods for calculation and assembly of the finite element matrices are briefly mentioned. An outline of the mesh generating algorithms is also presented. Validation of the solution is considered next. Capacitance of two canonical microstrip shapes, namely the circular and the rectangular is computed and compared with the values obtained from an integral equation solution, as well as with data obtained from a number of referenced sources. Finally, to illustrate the versatility of the SDFEM formulation, capacitance of more complicated microstrip geometries is calculated and presented in graphical form.

Conclusions are presented in Section IV, which also includes suggestions for future work.

Manuscript received August 27, 1990; revised July 30, 1992.

The authors are with the Department of Electrical Engineering, University of Minnesota, 200 Union St., S.E., Minneapolis, MN 55455.

IEEE Log Number 9206300.

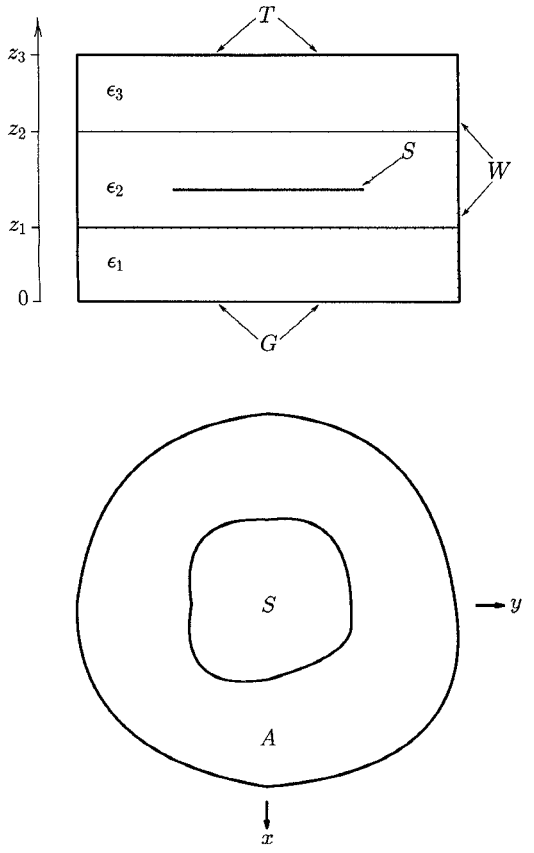

Fig. 1. Shielded microstrip patch in a stratified dielectric medium ($A, \partial A$—cross-section and its boundary, respectively).

II. Formulation of the Solution

A statement of the proposed problem, outlining the main assumptions, is presented in this section. The semi-discrete finite element method is introduced and applied to reduce the formulation to a form suitable for computation.

Consider a planar circuit element formed by a single conductive sheet embedded in a stratified dielectric medium, as shown in Fig. 1. The conductive strip is assumed to be infinitesimally thin, but otherwise no restriction is placed on its shape. The lateral extent of the dielectric is limited by a cylindrical metalic enclosure, which may have an arbitrary cross-section. Metalic plates, parallel to the dielectric interfaces, are introduced to terminate the structure on the top and the bottom. Later it will be shown that although numerical considerations dictate that the model have finite lateral dimensions, vertically it may extend to infinity in either direction. Moreover, the formalism introduced in this section can be used to extend the analysis to circuits composed of any number of dielectric layers and parallel metalic strips.

Problem Statement

In order to evaluate the capacitance of the circuit element shown in Fig. 1 it will be necessary to solve the following boundary value problem:

1. Poisson's equation in the nth layer:

$$\nabla^2\phi(x,y,z) = -\frac{1}{\epsilon_n}\rho(x,y,z) \tag{1}$$

where $\phi(x,y,z)$—potential ϵ_n—permittivity of the layer $\rho(x,y,z)$—charge density distribution

$$\rho(x,y,z) = \begin{cases} 0 & \text{if } n = 1,3 \\ \sigma(x,y)\,\delta(z-z') & \text{if } n = 2 \end{cases} \tag{2}$$

2. Boundary conditions:

$$\phi(x,y,z) = 0 \quad \text{if } (x,y,z) \in \text{W, T, G} \tag{3}$$

$$\phi(x,y,z) = \phi_0 \quad \text{if } (x,y,z) \in \text{S} \tag{4}$$

3. Transition conditions at the kth dielectric interface ($z = z_k$):

$$\phi(x,y,z_k^+) = \phi(x,y,z_k^-) \tag{5}$$

$$\epsilon_{k+1}\frac{\partial\phi}{\partial z}(x,y,z_k^+) = \epsilon_k\frac{\partial\phi}{\partial z}(x,y,z_k^-) \tag{6}$$

Solution of the posed problem yields $\sigma(x,y)$—the charge density distribution on the strip, from which the capacitance can be calculated using the following formula

$$C_s = \frac{Q}{\phi_0} \tag{7}$$

where Q is the total charge residing on the strip, i.e.

$$Q = \int_S \sigma(x,y)\,dx\,dy \tag{8}$$

Weak Form of the Problem Statement

In constructing finite element solutions it is common to abandon the differential equation statement of the problem in favor of the so-called weak or variational formulation [11]. The semi-discrete FEM differs from the so-called conventional methods in one key respect. In the semi-discrete approach one of the Cartesian coordinates is treated as a parameter and finite element discretization is introduced only on surfaces transverse to this coordinate. For the problem at hand the z-coordinate will serve as a parameter.

A weak formulation of (1) which will be used as the basis for subsequent numerical analysis seeks a function $\phi(x,y,z)$ which will satisfy

$$\int_A \left[-\nabla_t\phi\cdot\nabla_t\psi + \frac{\partial^2\phi}{\partial z^2}\psi + \frac{1}{\epsilon_n}\rho\psi\right] dx\,dy + \oint_{\partial A}\frac{\partial\phi}{\partial n}\psi\,dc = 0 \tag{9}$$

for all values of z and all weight functions $\psi(x,y)$ satisfying certain integrability conditions [11]. The integration domain in (9) is the cross-section A of the structure shown in Fig. 1. $\partial\phi/\partial n$ denotes the normal derivative of ϕ on the contour ∂A bounding the cross-section A, and ∇_t is the transverse (to z) gradient operator.

Finite Element Approximation

A combination of numerical and analytical methods will be utilized to obtain an approximate solution to (9). In the first stage of analysis, the cross-section A of the structure will be divided into a finite number of simply-shaped sub-domains or elements, collectively known as the finite element mesh. The details of mesh construction are considered in Section III.

After the cross-section A has been discretized the Galerkin method is implemented to construct an approximate solution to the problem. The sought solution is expanded in terms of the chosen basis set $\{\phi_i(x,y)\}_{i=1}^N$ as follows

$$\phi(x,y,z) = \sum_j v_j(z)\,\phi_j(x,y) = \tilde{\boldsymbol{\phi}}(x,y)\,\boldsymbol{v}(z) \tag{10}$$

where

$v_j(z)$—value of the approximate solution at (x_j, y_j, z),
(x_j, y_j)—coordinates of the jth node in the mesh,
$\phi_j(x,y)$—jth basis function,
$\boldsymbol{\phi}(x,y) = \text{vect}\{\phi_j(x,y)\}$,
$\boldsymbol{v}(z) = \text{vect}\{v_j(z)\}$,
and tilde denotes transposition.

The basis functions ϕ_i are generated using low-order polynomials, defined piecewise over the individual elements. Each basis function has a value of unity only at one node in the mesh and is zero at all other nodes, i.e., $\phi_j(x_i, y_i) = \delta_{jk}$, where (x_j, y_j) are coordinates of the kth node in the mesh and δ_{jk} is the Kronecker delta.

Substitution of (10) into the weak statement (9) and use of the functions $\{\phi_i(x,y)\}_{i=1}^N$ to test the resulting equation over the domain A, leads to the following system of N coupled, ordinary differential equations in the N unknowns $v_j(z)$

$$\boldsymbol{B}\frac{d^2\boldsymbol{v}(z)}{dz^2} - \boldsymbol{A}\boldsymbol{v}(z) = -\frac{1}{\epsilon_n}\boldsymbol{s}\delta(z-z') \tag{11}$$

where $\boldsymbol{v}, \boldsymbol{s}$ are $N \times 1$ vectors and $\boldsymbol{A}, \boldsymbol{B}$ are $N \times N$ sparse, symmetric and positive-definite matrices, whose elements are defined by the following equations

$$a_{ij} = \int_A \nabla_t\phi_i \cdot \nabla_t\phi_j\,dx\,dy \tag{12}$$

$$b_{ij} = \int_A \phi_i\phi_j\,dx\,dy \tag{13}$$

$$s_i = \int_A \sigma\phi_i\,dx\,dy \tag{14}$$

where $\sigma(x,y)$ is the surface charge density defined in (2).

Note that the boundary integral term in (9) does not contribute to (11)–(14). This has been accomplished by requiring that the weight functions have zero values on nodes located on the boundary ∂A of the cross-section. Thus, the boundary condition (2) on the lateral wall W (Fig. 1) is satisfied.

Solution of the ODE Set

Although a number of numerical methods can be applied to solve the set of ODE in (11), from the standpoint of numerical efficiency it is advantageous to maximize analytical processing in solving this equation. An expedient approach to use involves decoupling of the unknowns by a linear transformation of the solution $\boldsymbol{v}$ to the principal axis [7], followed by the analytical solution of the decoupled system, and subsequent retransformation to the original basis. Let

$$\boldsymbol{v}(z) = \boldsymbol{T}\boldsymbol{V}(z) \tag{15}$$

where $\boldsymbol{T}$ is a linear transformation and $\boldsymbol{V}(z)$ the transformed solution. After substitution of (15) into (11) it becomes clear that to decouple the unknowns, the matrix $\boldsymbol{T}$ must satisfy the following generalized eigenvalue problem

$$\boldsymbol{A}\boldsymbol{T} = \boldsymbol{B}\boldsymbol{T}\boldsymbol{K} \tag{16}$$

wherein the columns of $\boldsymbol{T}$ are the eigenvectors and $\boldsymbol{K} = \text{diag}(k_i^2)$ is a diagonal matrix whose entries k_i^2 represent the corresponding eigenvalues. The given eigenvalue problem can be solved numerically using well-established techniques and widely available software [12].

When (11) is transformed to the principal axis, it takes on the following form:

$$\frac{d^2\boldsymbol{V}(z)}{dz^2} - \boldsymbol{K}\boldsymbol{V}(z) = -\frac{1}{\epsilon_n}\hat{\boldsymbol{s}}\delta(z-z') \tag{17}$$

where $\hat{\boldsymbol{s}} = \boldsymbol{T}^{-1}\boldsymbol{B}^{-1}\boldsymbol{s}$.

This matrix equation corresponds to N uncoupled ordinary differential equations.

Transmission Line Analogy for (17)

Since the elemental equations in (17) have the same form and are independent, it suffices to examine one of them, e.g. the equation for $V_i(z)$. Aside from the constant $\hat{s}_i$ (the ith element of $\hat{\boldsymbol{s}}$) in the source term, there is formal similarity between the ith scalar equation in (17) and the Green function problem for a transmission line excited by a current unit point-source. It is convenient to exploit this similarity in generating solutions of (17). The methodology for solving transmission line Green function problems is well-known [13]–[15]. Therefore, an analogy between the variables appearing in (17) and the various transmission line parameters will permit its solution by inspection. Table I summarizes the correspondence used to establish the aforementioned analogy.

In order to apply transmission line analysis to the problem at hand, each dielectric stratification in Fig. 1 is modeled by a transmission line of appropriate characteristic impedance. The analog of the three-layer configuration in Fig. 1 is the model comprised of three cascaded transmission line sections. The first and the third are terminated in short circuits (metalic plates T, G), and the shunt point current source, representing the delta function term on the right-hand side of (17), is connected in the second section at $z = z'$. Additional constraints, analogous to (5), (6) and reflecting the continuity of voltage and current, must be applied at the junctions between lines of distinct characteristic impedance (dielectric interfaces).

The solution $V_i(z)$ to the ith differential equation in (17) follows directly from the transmission line Green function analysis, and Table I. Denoting the transmission line Green function evaluated with $k = k_i$ by $\hat{Z}_i(z,z')$, the solution can be expressed as follows

$$V_i(z) = \hat{Z}_i(z,z')\hat{s}_i \tag{18}$$

TABLE I
TRANSMISSION LINE ANALOGY FOR EQ. (17)

Variables in (19)	Transmission line parameters
$V_i(z)$	Voltage $V(z)$
$-\epsilon_n \dfrac{dV_i(z)}{dz}$	Current $I(z)$
$\dfrac{1}{k_i \epsilon_n}$	Characteristic impedance Z_{0n}
$k_i \epsilon_n$	Characteristic admittance Y_{0n}
k_i	Propagation constant k

where $\hat{s}_i$ is the ith element of the vector $\hat{\boldsymbol{s}}$ defined in connection with (17). In matrix notation the solution becomes

$$\boldsymbol{V}(z) = \hat{\boldsymbol{Z}}(z, z')\boldsymbol{T}^{-1}\boldsymbol{B}^{-1}\boldsymbol{s} \tag{19}$$

where $\hat{\boldsymbol{Z}}(z, z') = \text{diag}\{\hat{Z}_i(z, z')\}$.

The solution $\boldsymbol{v}(z)$ to the original set of ODE is obtained by transforming $\boldsymbol{V}$ into the original basis. Combining (15) and (19) results in

$$\boldsymbol{v}(z) = \boldsymbol{T}\hat{\boldsymbol{Z}}(z, z')\boldsymbol{T}^{-1}\boldsymbol{B}^{-1}\boldsymbol{s} \tag{20}$$

If the eigenvector matrix $\boldsymbol{T}$ is normalized according to $\tilde{\boldsymbol{T}}\boldsymbol{B}\boldsymbol{T} = \boldsymbol{I}$, where the tilde denotes transposition, (20) can be written as

$$\boldsymbol{v}(z) = \{\boldsymbol{T}\hat{\boldsymbol{Z}}(z, z')\tilde{\boldsymbol{T}}\}\boldsymbol{s} = \boldsymbol{Z}(z, z')\boldsymbol{s} \tag{21}$$

where $\boldsymbol{Z}(z, z')$ denotes the bracketed matrix product.

Application of Boundary Conditions and Calculation of Capacitance

The boundary conditions stated in (3) are applied at various stages in the development of the solution. The conditions on the lateral walls of the enclosure are incorporated into the framework of the finite element model of the transverse-to-z cross-section. The homogeneous Dirichlet condition on the top T and bottom G plates (which becomes the far-field condition when T, G are at infinity) is applied in the context of the solution for the coefficients $\boldsymbol{v}(z)$. The remaining boundary condition, i.e. the one on the microstrip metal S, will be enforced last. Completion of this step will make possible the calculation of the charge Q and the capacitance C.

To apply the boundary condition on the strip S, it is necessary to return to (10) and substitute into it the derived z-dependent coefficients. Then, letting $z = z'$ in equation (21), and applying the boundary condition (3) leads to the following equation

$$\begin{aligned} \boldsymbol{\phi}_0 &= \tilde{\phi}(x, y) \\ \boldsymbol{v}(z) &= \tilde{\boldsymbol{\phi}}(x, y)\,\boldsymbol{Z}(z', z')\boldsymbol{s} \quad \text{for all } (x, y, z') \in S \end{aligned} \tag{22}$$

Expression (22) can be reduced to a set of linear equations by enforcing the equality pointwise at all the nodes located on S. The final result will be a matrix equation for the M non-zero values of the vector $\boldsymbol{s}$, where M is the number of nodes in S.

The total charge Q is computed simply by summing all the elements of $\boldsymbol{s}$. The proof is straightforward

$$\begin{aligned} \sum_{m=1}^{M} s_m &= \sum_{m=1}^{M} \int_A \sigma(x, y)\,\phi_m(x, y)\,dx\,dy \\ &= \int_A \sigma(x, y) \overbrace{\left[\sum_{m=1}^{M} \phi_m(x, y)\right]}^{\equiv 1} dx\,dy \\ &= \int_A \sigma(x, y)\,dx\,dy = Q \end{aligned} \tag{23}$$

III. NUMERICAL CONSIDERATIONS

Mesh Generation

In all cases considered here the transverse cross-section A was partitioned into triangular elements. This choice affords versatility in the modeling of irregularly-shaped domains. Moreover, automatic generation and refinement of triangular element meshes can be implemented with relative ease. Distribution of the nodes—vertices of the elements—is governed by several considerations, most important of which is the local behavior of the solution. Intuitively, it is clear that regions where the solution varies rapidly (and its derivatives are large) require finer discretization, while portions of the domain with relatively slow, smooth variations can have coarser meshes. This point requires further elaboration in the case of the semi-discrete finite element method, in which only the transverse cross-section is discretized. In (9), the values of the potential on the mesh are functions not only of the coordinates x, y in the plane of the mesh, but of the vertical coordinate (z) as well. Therefore, when the cross-section A is discretized, the resulting mesh should be adopted to the features of the solution in a continuum of z = constant planes. It appears then, that the mesh geometry should change as a function of z. However, this is not possible in the context of the semi-discrete FEM. The way out of this dilemma is to tailor the mesh to a specific z = constant plane, namely the one in which the derivatives of the solution exhibit largest variation. In the structure shown in Fig. 1 this is the strip $(z = z')$ plane, because the second derivative of the solution is singular at the strip edge. A very finely graded mesh is required in these areas in order to minimize the error inherent in the piecewise-linear interpolation of the solution. In the implemented meshing algorithm, locations of the nodes were determined according to a specified formula, depending on the relative distances of a node to the outer walls and microstrip edges. The general criterion used, requires the inter-node distances to decrease approximately as the inverse square-root when approaching a metal boundary from either side.

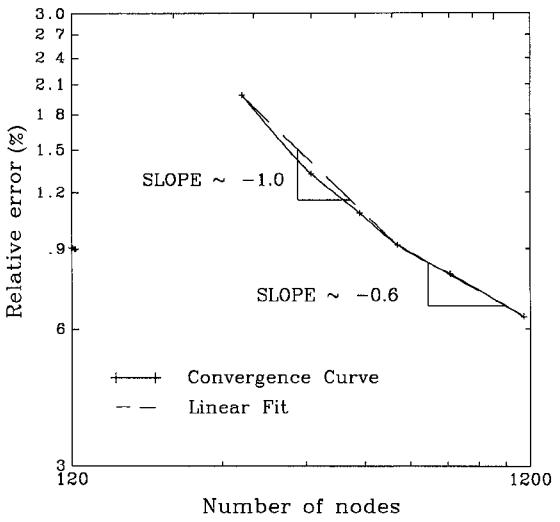

Fig. 2. Typical relative convergence curve.

Validation of the Solution

In (10) of the preceding section a set of basis functions was introduced to approximate the (x, y) variation of the potential. Numerical tests of the solution derived in that section were performed with piecewise-linear basis functions. Derivation of these and other types of basis functions, as well as the methods used for calculation and assembly of the matrices $\boldsymbol{A}, \boldsymbol{B}$ can be found in most introductory texts on the finite element method, e.g. [11], [16], and, therefore, will not be discussed here. It should be mentioned, however, that because all the finite element calculations, particularly the evaluation of the integrals in (12)–(14), can be carried out analytically, the time required to fill $\boldsymbol{A}, \boldsymbol{B}$ is negligible.

The convergence characteristics of the formulated finite element solution are summarized in Fig. 2. The case under study is that of a circular disk with substrate thickness-to-disk radius ratio $t_1/a = 1$, with air dielectric substrate. The enclosure-to-disk radius ratio $c/a = 10$. The reference value for relative error calculations is determined using the analytical formulas from [8]. Convergence is examined as a function of the total number of mesh nodes, i.e. the number of unknowns in the problem. The curve in Fig. 2 exhibits two distinct rates of convergence, depending on the number of nodes N. For smaller values of N the convergence is $O(1/N)$. For $N > 500$, the convergence rate appears to decrease, its behavior now characterized as $O(1/N^{0.6})$. Note, however, that the relative error at the point of convergence rate transition is less than 1%. It can be shown [11] that for an optimally distributed mesh, use of linear basis functions should in fact result in $O(1/N)$ convergence. The deviation from this behavior for large values of N can be attributed to poorer mesh control and roundoff errors associated with the solution of the eigenvalue problem stated in equation (16). Incidentally, the solution of this eigen-equation constitutes the bulk, 90% or greater, of the overall CPU time consumed.

Two microstrip geometries, namely the circular and the rectangular (square), were selected in order to test the accuracy of the solution. The primary reasons for this choice were: i) the availability of published data for comparison, and ii) the possibility of applying a different method to analyze these geometries and thus obtain another set of reference results.

Capacitance of a circular patch on a dielectric sheet in front of a ground plane has been the subject of numerous investigations. Wheeler [8] has combined the results of his own derivations with previously published expressions and numerical data to produce a highly accurate formula, valid for the entire range of substrate thickness-to-disk radius (t_1/a) and permittivity (ϵ_{r1}) values. The case of the disk in a multilayer dielectric environment has received less attention, and few data were found in literature. In order to verify the validity of the SDFEM for a wide range of configurations, including the later case, an integral equation was formulated for a disk in a cylindrical box containing stratified dielectric medium. The integral equation was solved by the Moment Method, employing suitable basis/testing functions. The details of the integral equation solution are omitted. In all cases, the results of calculations carried out with SDFEM will be compared with integral equation derived data, and, where appropriate, with values calculated from Wheeler's formula.

Capacitance of a rectangular and square disks in a general stratified medium has been computed by Bhat and Koul [2], using the variational approach with an approximate form of charge distribution on the strip. Additionally, as in the case of the circular disk, an integral equation was formulated and solved numerically.

Capacitance data for a circular disk on a single ground-backed dielectric sheet are plotted in Fig. 3 as a function of the ratio t_1/a, for several values of permittivity. Numerical studies of the integral equation solution indicate that it converges rapidly as the number of included modes in the Green function summation and the number of entire-domain basis/testing functions are increased. Therefore, data resulting from the integral equation solution are considered to be highly accurate. Comparison between these data (labeled by IE in Fig. 3) and capacitance values computed with SDFEM on a mesh which contained 1162 nodes shows a uniform discrepancy in the range of $.5 - .8\%$, the SDFEM results being consistently greater. Wheeler's formula yields data which confirm the accuracy of both the integral equation, as well as SDFEM, calculations for smaller t_1/a values. They diverge when t_1/a is large, because the configuration studied by Wheeler was infinite in lateral extent, whereas the other formulations included a metallic cylindrical wall. It was expected, and has been confirmed that the capacitance is unaffected by the walls presence, provided that that the ratio t_1/a is smaller than a certain number, which depends on the patch-to-wall distance and the permittivity of the dielectric. As indicated in the legend to Fig. 3, the SDFEM and integral equation capacitance calculations were performed with $c/a = 10$. In Fig. 4 the validity of SDFEM is verified for the case where the disk is embedded in a multilayer (substrate-superstrate) configuration. Again, the agreement with the integral equation results is very good, the difference remaining less than 0.7% throughout the entire range of geometrical and electrical parameters.

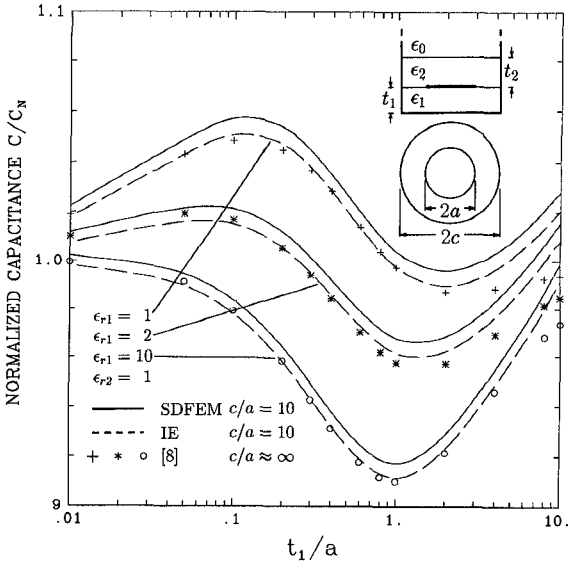

Fig. 3. Capacitance of a circular disk on a dielectric substrate—validation of the solution.

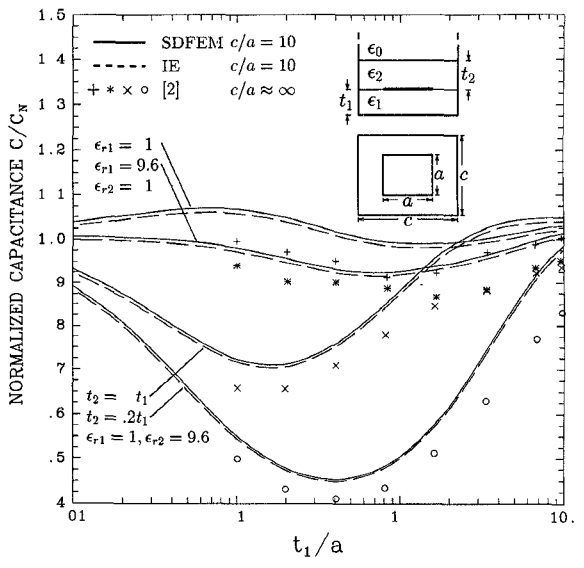

Fig. 5. Capacitance of a rectangular patch—validation of the solution.

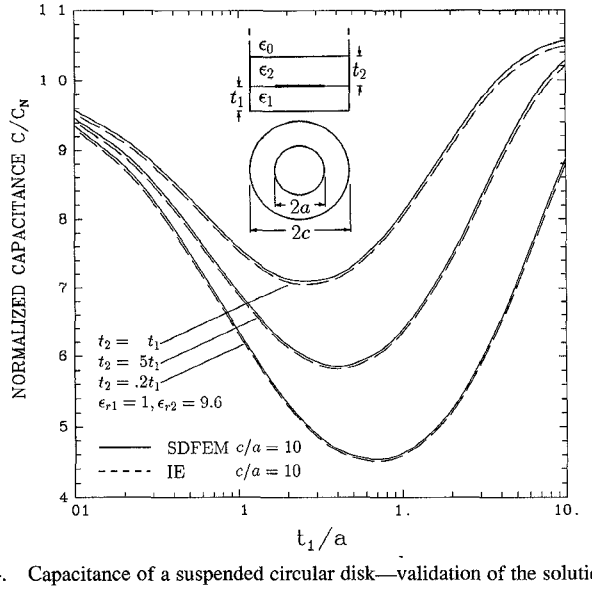

Fig. 4. Capacitance of a suspended circular disk—validation of the solution.

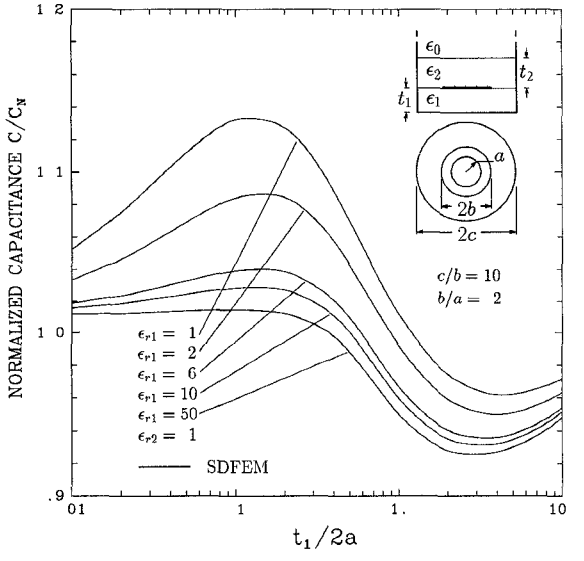

Fig. 6. Capacitance of an annular patch with circular boundaries.

An array of calculations similar to that performed for a circular disk was also carried out for the square microstrip patch. The results are displayed in Fig. 5. The data were obtained from three distinct sources, i.e. SDFEM method with 956 nodes, integral equation formulation and reference [2]. Most of the discussion pertaining to the circular disk remains valid for the square path. The discrepancy between SDFEM and the integral equation calculations is in all instances less than 0.8%. The capacitance values acquired from the graphs in [2] are typically $5-7\%$ lower, with $1-2\%$ attributable to the device used to digitize the graphs.

Finally, to demonstrate the versatility of the SDFEM solution, capacitances of patches with more complex, annular geometries were calculated. In the first case the annulus is bounded by two concentric circles, whereas in the second case the outer boundary is an equilateral triangle. While it may still be possible to find appropriate basis functions and solve the integral equation for the circular annulus, doing so for the compound triangular-circular geometry would be very difficult. On the other hand, the SDFEM solution is uniformly applicable to such, and potentially more complex, geometries. Capacitance of the 2 : 1 circular annulus is displayed in Fig. 6 as a function of the substrate thickness-to-outer circle radius ratio (t_1/b), for a number of substrate permittivities. In Fig. 7 the capacitance of the triangular-circular annulus is plotted as a function of the substrate thickness-to-inner circle diameter $(t_1/2a)$.

In order to facilitate comparison between various solutions, the capacitance values in Figs. 3–7 were normalized by specific expressions (C_N), listed in Table II. The formulas given in Table II represent sums of the capacitances for the two asymptotic limits of the patch-to-ground plane spacing, namely zero and infinity.

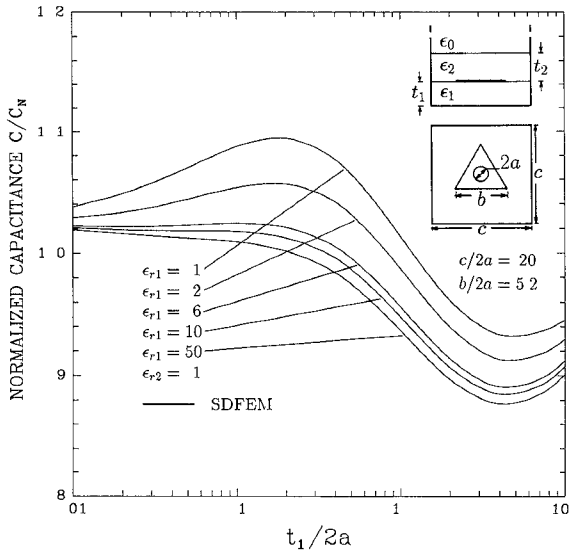

Fig. 7. Capacitance of an annular patch with an equilateral-triangular outer and circular inner boundaries.

TABLE II
NORMALIZATION CAPACITANCE C_N

Figure #	C_∞	Patch area A
4	$8.0a$	πa^2
5	$8.0a$	πa^2
6	$4.7a$	a^2
7	$8.4b$	$\pi(b^2 - a^2)$
8	$37.2a$	$0.433b^2 - \pi a^2$

IV. CONCLUSIONS

The Semi-Discrete Finite Element method was used to analyze a static formulation for a class of microstrip components. Among the demonstrated features of the SDFE method are versatility—applicability to microstrip patches with arbitrary metallization boundaries and ease of formulation and coding. Comparison of the results obtained using the SDFE method with data obtained from other solutions was used to validate the method.

REFERENCES

[1] A. Farrar and A. T. Adams, "Computation of lumped microstrip capacities by matrix methods," *IEEE Trans. Microwave Theory Tech.*, vol. MTT-20, p. 294, Apr. 1972.
[2] B. Bhat and S. K. Koul, "Lumped capacitance open-circuit end effects, and edge-capacitance of microstrip transmission lines," *IEEE Trans. Microwave Theory Tech.*, vol. MTT-32, no. 4, pp. 433–439, Apr. 1984.
[3] R. R. Boix and M. Horno, "Lumped capacitance and open end effects of striplike structures in multilayered and anisotropic substrates," *IEEE Trans. Microwave Theory Tech.*, vol. 37, no. 10, pp. 1523–1527, Oct. 1989.
[4] R. R. Boix and M. Horno, "Capacitance computation of elliptic microstrip disks in biaxial anisotropic multilayerd substrates," *IEEE Trans. Microwave Theory Tech.*, vol. 38, no. 1, pp. 30–37, Jan. 1990.
[5] A. K. Sharma and B. Bhat, "Spectral domain analysis of elliptic microstrip disk resonators," *IEEE Trans. Microwave Theory Tech*, vol. MTT-28, no. 6, pp. 573–576, June 1980.
[6] W. C. Chew and J. A. Kong, "Effects of fringing fields on the capacitance of circular microstrip disk," *IEEE Trans. Microwave Theory Tech.*, vol. MTT-28, pp. 98–104, Feb. 1980.
[7] R. Pregla and W. Pascher, "The method of lines," ch. 6, *Numerical Techniques for Microwave and Millimeterwave Passive Structures*, T. Itoh, Ed., New York: Wiley Interscience, 1989.
[8] H. A. Wheeler, "A simple formula for the capacitance of a disk on dielectric on a plane," *IEEE Trans. Microwave Theory Tech.*, vol. MTT-30, no. 11, pp. 2050–2054, Nov. 1982.
[9] L. V. Kantorovich and V. I. Krylov, *Approximate Methods of Higher Analysis*. New York: Interscience, 1958.
[10] D. C. Zienkiewicz, *The Finite Element Method*. New York: McGraw-Hill, 1977.
[11] E. B. Becker, G. F. Carey, J. T. Oden, *Finite Elements. An Introduction*. Englewood Cliffs, NJ: Prentice-Hall, 1981.
[12] B. T. Smith *et al.*, *Matrix Eigensystem Routines: EISPACK Guide*. New York: Springer-Verlag, 1976.
[13] W. L. Weeks, *Electromagnetic Theory for Engineering Applications*. New York: Wiley, 1964.
[14] P. E. Mayes, *Electromagnetics for Engineers*, published by author, 1965.
[15] L. Felsen and N. Marcuvitz, *Radiation and Scattering of Waves*. Englewood Cliffs, NJ: Prentice-Hall, 1973.
[16] D. S. Burnett, *Finite Element Analysis: from Concepts to Applications*. Reading, MA: Addison-Wesley, 1988.
[17] P. M. Morse and H. Feshbach, *Methods of Theoretical Physics*. New York: McGraw-Hill, 1953.
[18] W. R. Smythe, *Static and Dynamic Electricity*, 3rd ed., rev. printing, New York: Hemisphere Pub. Corp., 1989.
[19] R. F. Harrington, *Field Computation by Moment Methods*. New York: Macmillan, 1968.

Marat Davidovitz (S'81–M'81) received the B.S. (Highest Honors) and M.S. degrees in electrical engineering from the University of Illinois, Chicago, in 1981 and 1983, respectively, and the Ph.D. degree in electrical engineering from the University of Illinois, Urbana-Champaign, in 1987.

Throughout his graduate studies he was employed as a Research and Teaching Assistant. From 1987 to 1988 he was an Alexander von Humboldt post-doctoral fellow at DLR, Oberpfaffenhofen, Germany. In the Fall of 1988 he joined the Department of Electrical Engineering, University of Minnesota, Minneapolis as an Assistant Professor. Among his interests are microstrip circuits and antennas, electromagnetic scattering and applied numerical analysis.

Zhiqiang Wu (S'92), photograph and biography not available at the time of publication.